# Implications of posture changes on local SAR and B1+ homogeneity in RF shimming at 3T

Desmond Teck Beng Yeo[1], Zhangwei Wang[2], and Ileana Hancu[1]
[1]*Diagnostics and Biomedical Technologies, GE Global Research, Niskayuna, NY, United States,* [2]*GE Healthcare Coils, Aurora, OH, United States*

**Introduction**: The advent of high-field MRI has led to the development of multi-channel transmit RF coils, which afford more degrees of freedom to tailor $B_1^+$ and E-field distributions. The prediction of local SAR in multi-channel transmit systems is a highly challenging task. One approach involves using EM simulations to calculate SAR distributions after optimizing the voltage feeds' complex weights to obtain uniform excitation profiles. The optimized weights are then applied to the input of the RF power amplifiers and the transmitted waveforms are monitored [1-3]. If the transmitted waveforms correlate with the calculated waveforms, an estimate of the local SAR distribution is deemed to be available from the simulations. This approach provides some information about local SAR risks, especially if a patient- and position-specific human body model (HBM) is used. However, when a subject moves [4,5] after RF shimming optimization, the complex weights calculated for the previous posture may no longer apply. Our work uses EM simulations and a posable HBM to investigate $B_1^+$ homogeneity and peak local $SAR_{10g}$ variations when a subject moves after 3T RF shimming optimization is performed for an initial posture.

**Methods:**

***FDTD modeling***: A 16-rung TEM body coil (dia. 61.0cm, length 42.2 cm) connected to a RF shield (dia=65.0cm, length=100.0cm) via copper strips (2.5cm×2.0cm) is modeled and tuned to 127.74MHz with SEMCAD X (SPEAG, Zurich, Switzerland). Each rung is excited with an independent 50 Ω voltage source at 127.74 MHz with adjustable amplitude and phase. The tuning is done by feeding a broadband Gaussian pulse to one voltage source at a time while the capacitors of the respective rung are varied [6]. Each TEM rung is 2.5cm wide, 42.2cm long, and has four capacitor junctions. In circularly polarized mode, the voltages sources have equal magnitudes and azimuthally dependent phases (22.5° apart in adjacent rungs). The 'Duke' (77 tissue types, weight:72.4 kg, height:1.77m) human body model (HBM) from the "Virtual Family" dataset [7] is used in the experiments. Using the Poser software (SPEAG, Zurich, Switzerland), four different HBM postures (P0 to P3) are created with the pelvises located in the center of the rungs (Fig. 1). The back of the HBM is located 175mm away from the furthest rung in the posterior direction. The 4 models are meshed to a minimum finite-difference time-domain (FDTD) cell size of 3mm×3mm×3mm. A 4-Cole-Cole extrapolation method is used to compute the electrical properties of the various tissue types.

***RF shimming:*** The TEM coil rungs are individually excited to obtain 16 sets of complex $B_1^+$ maps of the HBM in posture P0. Using Matlab (Mathworks, Natick, MA), the 16 $B_1^+$ maps from the same axial slice (isocenter of coil) are linearly combined with optimal complex weights calculated by three RF shimming approaches (max-min, phase-only [8], amplitude-phase [9,10]) using the following cost functions:

$$\Psi_{\max-\min}(\mathbf{w}) = \sum_{\mathbf{r}} \left( 1 / \left| \sum_{k=1}^{N} w_k B_{1,\mathrm{ch}\,k}^{+}(\mathbf{r}) \right| \right), \quad \Psi_{\text{phase}}(\mathbf{w}) = \left\| \underline{\mathbf{B}}_{1,\text{measured}}^{+} \mathbf{w} - \mathbf{B}_{1,\text{target}}^{+} \right\|^2 \text{ subject to } |w_n| = \text{constant for all channels, and } \Psi_{\text{amp-phase}}(\mathbf{w}) = \left\| \underline{\mathbf{B}}_{1,\text{measured}}^{+} \mathbf{w} - \mathbf{B}_{1,\text{target}}^{+} \right\|^2,$$

where $\mathbf{r}$ is the spatial coordinate vector, $\mathbf{w}$ is the vector of complex weights, $\underline{\mathbf{B}}_{1,\text{measured}}^{+}$ is a M×N matrix of individually excited $B_1^+$ values (column stacked) from EM simulations, $\mathbf{B}_{1,\text{target}}^{+}$ is a M×1 column-stacked vector of a desired $B_1^+$ profile, and M is the number of voxels in the RF shimming region. The optimal weights calculated for P0 are then applied to postures P1 to P3 in full-wave simulations to obtain peak $SAR_{10g}$ and $B_1^+$ homogeneity values. The resultant peak $SAR_{10g}$ values in P1 to P3 denote the SAR risks to the HBM if it moves after RF shimming optimization is done for an initial posture (P0). $B_1^+$ homogeneity values are defined as the mean of $B_1^+$ divided by the standard deviation $B_1^+$ in the axial slice of the HBM (excluding free space voxels).

***Experiments***: Forty simulations are performed (4 postures×[1 azimuthal+3 RF shimming techniques×3 RF shimming trials]). All computations were performed on an Intel Xeon quad-core 2.13 GHz CPU with two Nvidia Quadro FX5800 GPUs.

**Results and Discussion**: Each cell in Fig. 1 shows the average (over three RF shimming realizations) peak $SAR_{10g}$ and $B_1^+$ homogeneity values and their coefficients of variation (CV=σ/μ×100%) for each combination of posture and RF shimming algorithm. The CVs for the peak $SAR_{10g}$ values are much higher (>25%) for the phase and amp-phase RF shimming algorithms than for the $B_1^+$ homogeneity values. This is largely because the RF shimming algorithms seek to yield the highest $B_1^+$ homogeneity and do not take into account the associated E-fields (SAR) generated. Thus, values for the former are more consistent while the peak $SAR_{10g}$ variation is larger. The $B_1^+$ homogeneity is observed to increase from left to right in Fig. 1 as the number of degrees of freedom (amplitudes and phases) increases. Fig. 2(a) and 2(b) plot the average absolute *changes* in peak $SAR_{10g}$ and $B_1^+$ homogeneity for different postures and RF shimming algorithms as a percentage of the values calculated for posture P0. For any given RF shimming algorithm, higher percentage changes denote greater risks in relying on peak $SAR_{10g}$ and $B_1^+$ homogeneity values that are calculated for P0, i.e., values for P0 are no longer good predictors of local SAR risk and $B_1^+$ homogeneity. The changes in peak $SAR_{10g}$ are all greater than 30% except in one case (P3 phase-only). In contrast, the changes in $B_1^+$ homogeneity are all smaller than 30% except in two cases (P3 phase-only and phase-amp). This suggests that patient motion that occurs after RF shimming optimization can significantly alter the local SAR risks even when $B_1^+$ homogeneity appears relatively unchanged. However, it is possible that some postures may induce more significant changes to $B_1^+$ homogeneity values than others, e.g., P3 yielded at least one case where the change is >50%.

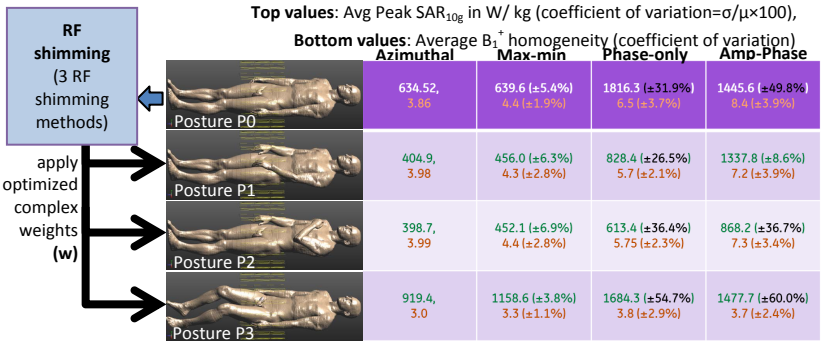


**Fig. 1.** Results of peak $SAR_{10g}$ and $B_1^+$ homogeneity when RF shimming weights calculated for posture P0 are applied to postures P1 to P3 (target of avg $B_1^+$=7uT in axial slice of pelvis). Three realizations of RF shimming weights were computed for each cell in the top row (except azimuthal case) and applied to postures P1 to P3 to generate data in rows 2 to 4. Each cell lists the average peak $SAR_{10g}$ value followed by the average $B_1^+$ homogeneity.

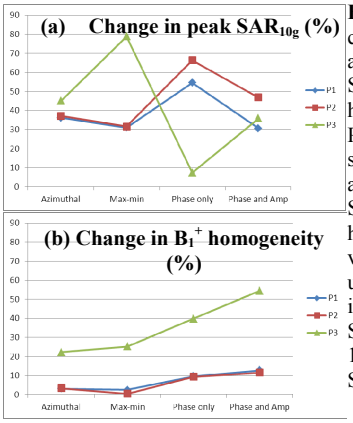


**Fig. 2**. Percentage changes in absolute (a) peak $SAR_{10g}$ and (b) $B_1^+$ homogeneity for P1 to P3 for all RF shimming algorithms. Peak $SAR_{10g}$ and $B_1^+$ homogeneity values for P0 are used as references, i.e., change in $SAR_{10g}$ (%) = $100\times|SAR_{P1} - SAR_{P0}|/ SAR_{P0}$

**Conclusions:** For the Duke HBM, posture changes after RF shimming optimization can result in significant variation in peak local $SAR_{10g}$ values, even when $B_1^+$ homogeneity values remain relatively unchanged. Since E-fields cannot be easily measured with MR, this implies that the SAR risks to the subject would change even if the operator continues to observe homogeneous $B_1^+$ maps after RF shimming has been performed at least once.

**References:** [1] Graesslin I, et al. ISMRM 2007 pg. 1086. [2] Brote I, et al. ISMRM 2009 pg. 4788. [3] Stang PP, et al. ISMRM 2009 pg. 3024. [4] Bammer R, et al. ISMRM 2011. [5] Graesslin I, et al. ISMRM 2007 p.867. [6] Yeo D, et al. JMRI 2011;33:1209-17. [7] Christ A, et al. 2010;55:N23–38. [8] Metzger GJ, et al. MRM 2008;59:396–409. [9] Hoult DI, et al. JMRI 2000;12:46-67. [10] Ibrahim TS, IEEE TMI 2006;25:1341-7.